Experimental study of a novel centrifugal compressor with two successive and independent rotors

Van-Thang NGUYEN[*]

Arts et Metiers Institute of Technology
CNAM, LIFSE, HESAM University
F-75013 Paris, France.
Email: thang.nguyen@ensam.eu

Cheikh Brahim ABED [†]

Arts et Metiers Institute of Technology
CNAM, LIFSE, HESAM University
F-75013 Paris, France.
Email: abedcheikhbrahim@gmail.com

Amelie DANLOS[‡]
Florent RAVELET
Richard PARIDAENS
Michael DELIGANT
Sofiane KHELLADI
Farid BAKIR

Arts et Metiers Institute of Technology
CNAM, LIFSE, HESAM University
F-75013 Paris, France

Abstract

The present study deals with a low pressure-ratio centrifugal compressor consisting of two counter-rotating rotors called a Counter-Rotating Centrifugal Compressor (CRCC). The design method based on the loss model was presented to determine the geometric parameters of the two counter-rotating rotors. According to this method, the rotor of a selected Single Rotor Centrifugal Compressor (SRCC) has been redesigned into two counter-rotating rotors (upstream and downstream rotors) by choosing the value of meridional Length Ratio (LR). The meridional view, the volute shape, and the operating parameters of SRCC are preserved during the design process. In a first step, the counter-rotating mode at a constant rotor speed of 11k rpm has been carried out. The overall characteristics of CRCC are compared to those of SRCC. In a second step, the map-characteristic of CRCC is established for seven speed ratios. The results show that CRCC increases up to 4,6% for the pressure ratio and 3.5% for the efficiency compared to SRCC at the same tip-speed. In addition, CRCC can operate at a lower tip-speed by about 2k rpm to produce the same characteristics as SRCC, with better efficiency over a wide range of flow rates. However, the surge margin of the CRCC is shifted to higher flow rates. This disadvantage of the CRCC was solved by choosing the adequate pair of the rotational speeds of the two rotors that will be presented in other publication.

Nomenclature

Symbols

- D Diameter of pipe, $D = 158.5mm$;
- d Diameter of rotor, m;
- k Coefficient of flow meter, k=0,72[-];
- ΔP Differential pressure of flow meter [Pa];
- ρ Gas density $[kg/m^3]$;
- Π_s Static pressure ratio [-];
- P Static pressure, [Pa];
- Δh The specific work/work done, Total enthalpy rise, $[J/kg]$;
- U Blade velocity, $[m/s]$;
- W Relative velocity, $[m/s]$;
- C Absolute velocity, $[m/s]$;
- T Temperature, $[K]$;
- N Rotational speed of rotor, $[rpm]$;
- Z Number of blade,[-];
- γ Specific heat rate [-];

[*]Faculty of Vehicle and Energy Engineering, Le Quy Don Technical University, 11917 Hanoi, Vietnam. Corresponding author

[†]École Supérieure Polytechnique, School of Engineering, BP 4303 Cite Cadres - Sebkha, Nouakchott - Mauritania.

[‡]Address all correspondence for other issues to this author.

$\dot{m}$ Mass flow rate, $[kg/s]$;
θ Speed ratio, $[\theta=\frac{N_{UR}}{N_{DR}}]$;
β Relative fluid flow angle, $[^\circ]$;
α Absolute fluid flow angle, $[^\circ]$;
β_b Blade angle, $[^\circ]$;
ϕ Stage flow coefficient, $[-]$;
η Efficiency, $[-]$;
I Work input coefficient, $[-]$;
L_B Blade camberline length, $[m]$;
m Meridional length, $[m]$;
ζ Non-dimensional meridional length, $[-]$;
L_{ax}, z Axial length, axial coordinate, $[m]$;
b Blade height, $[m]$;
t_b Blade thickness, m;
A Area, m^2;
BL Blade loading, $[-]$;
B Blockage factor, $[-]$;
σ Slip factor, $[-]$;
R Gas constant,$[J/kgK]$;
C_p Heat capacity,$[J/kgK]$;

Subscripts

m Meridional direction;
u Peripheral direction;
u Peripheral direction;
ref Reference condition;
cr Corrected condition;
u Peripheral direction;
h Hub;
s Shroud;
t Total condition;
1 Compressor inlet;
2 Upstream-rotor outlet;
3 Downstream-rotor inlet;
4 Downstream-rotor outlet;
5 Volute outlet;
b Blade;
par Parasitic;
p Polytropic condition;
atm Atmospheric;

abbreviation

$CRCC$ Counter-Rotating Centrifugal Compressor;
UR Upstream-Rotor;
DR Downstream-Rotor;
$SRCC$ Single Rotor Centrifugal Compressor;
HEP High Efficiency Point;
BEP Best Efficiency Point;

1 Introduction

A counter-rotating system comprises two successive rotors designed to follow opposite directions of rotation. This configuration has been used in almost families of turbo machines including for axial, centrifugal or mixed type machines pump [1–10]. The major advantage of the application of this system is the increase in power density. Many publications deal with using counter-rotating on turbomachine have been published including various patents [11,12], however, its application on a centrifugal compressors is not available in the open literature. In 2018, Dujour et al. [13] assessed by numerical simulations a non-axial counter-rotating configuration which cannot be described as a "counter-rotating centrifugal compressor" because the outlet flow is in the axial direction. This configuration gives a significant increase in pressure with almost no change in efficiency. The additional freedom offered by choosing of the two speeds of the upstream and downstream rotors allow further control and improve these counter-rotating machines performance over the extended operating range. The speed ratio is defined by the ratio of the upstream-rotor speed (N_{UR}) to the downstream-rotor speed (N_{DR}) was used to study this type of turbomachine.

$$\theta = \frac{N_{UR}}{N_{DR}} \tag{1}$$

Sharma et al. [3] studied many parameters that affect the performance of counter-rotating axial compressors, including speed ratios. Their results showed that if the downstream-rotor rotates 50% faster than the upstream-rotor, the rotation stall on the upstream-rotor is suppressed. In 2007, Furukawa et al. [4] conducted an experimental study of counter-rotating axial pumps. They found that the maximum efficiency could be archived at different mass flow rates when the speed ratio changed and the speed of the upstream-rotor is constant. The authors concluded that using the counter rotating component could give a wider operating range and a higher efficiency according to the speed ratio. To emphasize the effect of the speed ratio on the efficiency of the axial counter-rotating compressor, the work of Chen et al. [5] pointed out that with a speed ratio of 1.143, the compressor can achieve the highest efficiency with a slight reduction of the total pressure ratio and the working margin. They concluded that if the speed ratio is inferior to one, a stable range of the compressor becomes smaller and decreases when the speed ratio decreases. In 2012, the study of Limin et al. [14] presented that with a speed ratio higher than 0.9, the first stall stage appears in the downstream-rotor with a reduction of mass flow rate. In contrast, when the downstream-rotor rotates slower than the upstream-rotor, the tip leakage flow of the downstream-rotor decreases significantly with the decrease of the speed ratio. The stall phenomenon firstly occurs in the upstream-rotor. The study of Mistry et al. [15] on an axial counter-rotating fan showed that the speed ratio plays an important role in terms of overall pressure rise. When the downstream-rotor rotates faster than the first one, the suction effect is generated stronger. This improves the fan performance. Similarly, the study conducted by Nouri et al. [16] showed that the low-speed ratios give lower performances. Increasing the speed ratio within the range of [0.8 1.2] results in a slight increase in performance. The efficiency can reach a maximum value if it is in a range of [1.05 1.15]. The work of Subbarao et al. [17] on the speed ratio of a counter-rotating turbine shows that the overall efficiency is improved with a speed ratio greater than one. In addition,

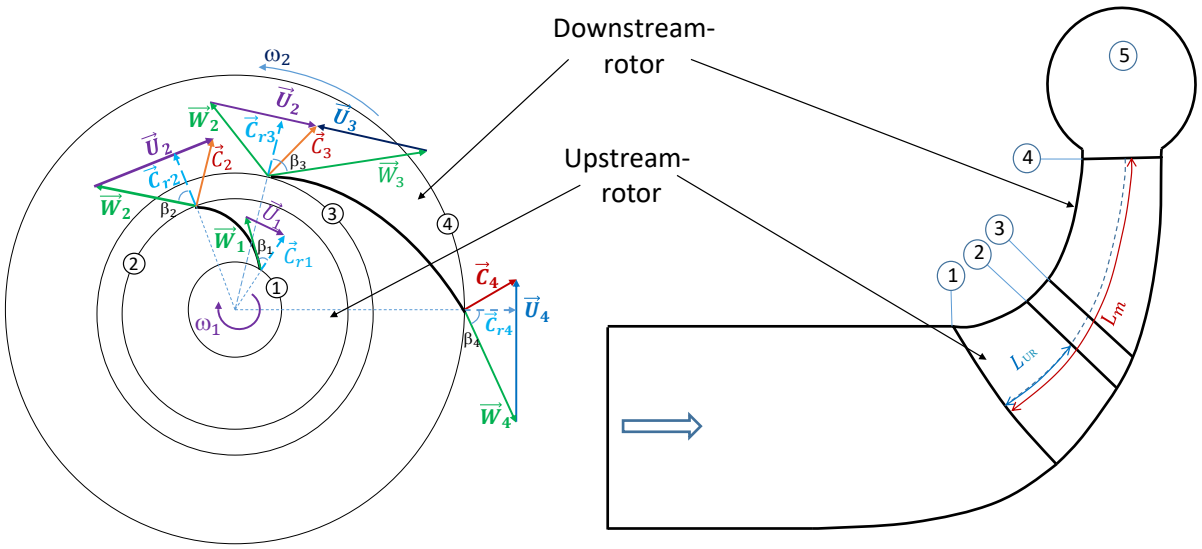

Fig. 1. Velocity triangle (a) and a meridional contour (b) were used to design CRCC. Points 1 and 2 represent the inlet and outlet of the downstream-rotor,respectively, and points 3 and 4 respectively stand for the inlet and outlet of the downstream-rotor. Points 5 represents the volute outlet

they identified that the losses vary with the speed ratio and that performance can be improved by adjusting the rotation speed of the rotors. In 2015, the experimental study of the counter-rotating mixed-flow pump was conducted by Tosin et al. [2] showed that the speed ratio has a powerful effect on the modification of entire pump characteristics. Their study focuses on the improvement of the head and on the optimization of the efficiency by changing the speed ratio. Experimental results showed that the head is changed from 12 to 26 m when the rotor has a higher rotation speed. The efficiency of the pump is almost constant at 80%. They also emphasize that the head rise is significantly improved by increasing the speed of the downstream-rotor while reducing the speed of the upstream-rotor. In this paper we present, for the first time in the literature, a design method for the two rotors of a CRCC. The experimental results obtained on a designed and produced machine in the laboratory are analyzed. This compressor confirms its superiority in power density and efficiency values over a wide operating range. A comparison with the available experimental characteristics of another conventional centrifugal compressor of the same size is provided in order to illustrate the superiority of CRCC.

2 Design of CRCC rotors

2.1 Velocity triangles of CRCC

The first step in the design method for CRCC is the presentation of the velocity triangles which are shown in figure 1. Apply the Euler equation for this case to determine the enthalpy of each rotor as well as the total enthalpy of the compressor as following relations:

$$\Delta h_1 = U_2 C_{u2} - U_1 C_{u1} \tag{2}$$

$$\Delta h_2 = U_4 C_{u4} - U_3 C_{u3} \tag{3}$$

Because of the counter-rotating effect, the component C_{u3} is negative and the upstream-rotor is considered no prewhirl ($C_{u1} = 0$). Consequently, the total enthalpy of CRCC is determined as:

$$\Delta h_{total} = U_4 C_{u4} + U_3 C_{u3} + U_2 C_{u2} \tag{4}$$

Obviously, the total enthalpy of CRCC is consistently higher than that of SRCC because two components $U_3 C_{u3}$ and $U_2 C_{u2}$ were added. As a result, CRCC configuration gives more pressure rise.

However, the main disadvantage of CRCC compared to SRCC is the relative velocity at the leading edge of the downstream-rotor. Indeed, this velocity increase dramatically by the counter-rotating effect as described in equation 5. The increase of this velocity can induce the choke of CRCC, and it should be paid attention in the design process considering the desired choke margin.

$$W_{u3} = U_3 + C_{u2} \ , \ W_3 = \sqrt{{C_{m3}}^2 + {W_{u3}}^2} \tag{5}$$

The designer should pay attention to this problem in CRCC design step to avoid the stage chocking and having an acceptable chock margin.

2.2 Design method for CRCC

In this study, the meridional shape of CRCC is kept the same as that of SRCC with the same volute for a fair comparison. Also, the leading and trailing edges of CRCC are

Table 1. Geometric parameters of SRCC

Parameter	Value	Parameter	Value
d_{1h}	59.5 mm	β_{b1h}	45.3°
d_{1sh}	161 mm	β_{b1sh}	69.8°
d_2	286 mm	β_{b2}	64°
b_2	29.7 mm	Z	7+7
N	16000 rpm	L_m	104.5 mm

also the same as that of SRCC, so only the counter-rotating effect will be properly investigated. The geometric parameters and the performance map of SRCC are shown in table 1 and figure 2.

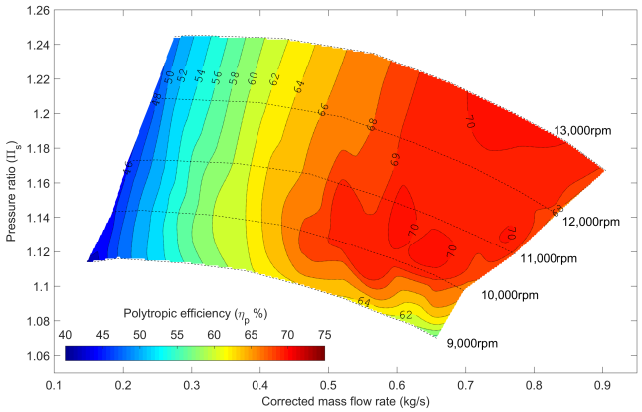

Fig. 2. Performance map of SRCC with $N \in [9k\,rpm,\ 13k\,rpm]$

The key to designing CRCC when its leading and trailing edges are fixed is to determine the position of the interface between the rotors, the trailing edge of the upstream-rotor and the leading edge of the downstream-rotor. To design CRCC, the single rotor of SRCC is divided into two separated rotors (upstream-rotor and downstream-rotor). The position of the interface between upstream and downstream-rotor is determined by the meridional Length Ratio (LR) which is defined by the following relation:

$$LR = \frac{L_{UR}}{L_m} \tag{6}$$

This parameter indirectly specifies the amount of the specific head that each rotor should deliver according to the total head offered by CRCC. Once LR is fixed, the upstream and downstream rotors can be calculated taking into account that the upstream-rotor inlet, the downstream-rotor outlet, and their meridional shape is already known. The downstream-rotor is directly determined after calculating the upstream-rotor by considering zero-incidence at the downstream-rotor leading edge by using equation 5.

For the design of the upstream-rotor, the iterative method of Aungier [19] is applied and coupled with the performance prediction method utilizing a combination of loss models. This method uses an empiric prediction of the Cordier line for optimum machines as a function of flow coefficient to predict the total head and calculate iteratively the blade angle and blade number based on a criterion on the global blade loading. The prediction of the Cordier optimal line is quite accurate compared to another empiric method as shown by Casey et al. [20]. Pakle et al. [21] have successfully implemented this method in order to design a high-performance centrifugal compressor. This method was also coupled with optimization techniques and used to optimize turbochargers as shown in Ref. [22]. Table 2 and 3 show a validation of the design code against two known existing single rotor stages. Figure 3 shows a validation of the loss model collection used in this study against experimental data of an open-source conventional centrifugal compressor and compared with the Oh's model [18].

Table 2. Geometrical parameters comparison between the developed code and the original centrifugal compressor-GT15V44 [23]

Description	Parameter	Original	Code
Shroud radius	r_{s1}	15.55 mm	14.155 mm
Shroud inlet blade angle	β_{bs1}	$-60°$	$-56.8°$
Outlet radius	r_2	22 mm	21.135 mm
Outlet blade height	b_2	2.66 mm	2.511 mm
Outlet blade angle	β_{b2}	$-45°$	$-45.339°$
Blade number	Z	6/6	12

Table 3. Geometrical parameters comparison between the developed code and the original centrifugal compressor-NASA CC3 [24]

Description	Parameter	Original	Code
Shroud radius	r_{s1}	105 mm	107.32 mm
Shroud inlet blade angle	β_{bs1}	$-56,536°$	$-55.625°$
Outlet radius	r_2	215.5 mm	210.7 mm
Outlet blade height	b_2	17 mm	17.4 mm
Outlet blade angle	β_{b2}	$-50°$	$-46.734°$
Blade number	Z	15/15	20

Thereby, the iterative design method is implemented for the upstream-rotor as:

$$\phi = \frac{\dot{m}}{\pi \rho_{t1} r_2^2 U_2} \tag{7}$$

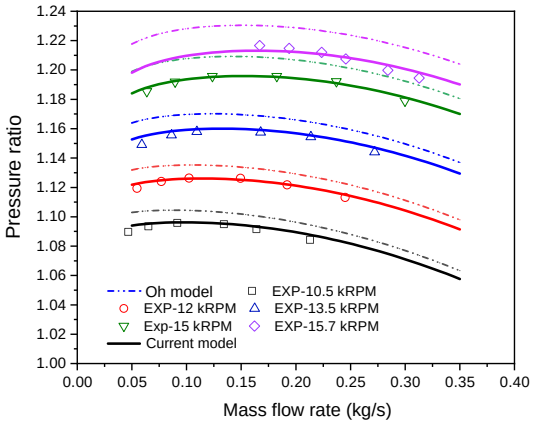

Fig. 3. Loss model validation against experimental data of KIMM SRCC and Oh's model [18]

$$I = \frac{\Delta h}{U_2{}^2} = 0.68 - \left(\frac{\phi}{0.37}\right)^3 + \frac{0.002}{\phi} \tag{8}$$

The parasitic losses are given by:

$$I_{par} = \frac{0.002}{\phi} \tag{9}$$

The internal polytropic efficiency of the rotor is given by:

$$\eta_p = 0.95 - \frac{0.0005}{\phi} \tag{10}$$

Absolute flow angle at trailing edge is determined as:

$$\tan(\alpha_2) = \frac{1}{0.26 + 3\phi} \tag{11}$$

Assuming zero pre-swril at the inlet of upstream-rotor, the tangential and meridional components of absolute velocity can be calculated respectively as:

$$C_{u2} = U_2(I - I_{par}) \tag{12}$$

$$C_{m2} = \frac{C_{u2}}{\tan(\alpha_2)} \tag{13}$$

The outlet total and static temperatures are calculated as:

$$T_{t2} = T_{t1} + \frac{\Delta h}{C_p} \tag{14}$$

$$T_2 = T_{t2} - \frac{C_2{}^2}{2C_p} \tag{15}$$

The outlet total and static pressure are calculated as:

$$P_{t2} = P_{t1}\left(1 + \frac{\eta_p(I - I_{par})U_2{}^2}{C_p T_{t1}}\right)^{\left(\frac{\gamma}{\gamma-1}\right)} \tag{16}$$

$$P_2 = P_{t2}\left(\frac{T_2}{T_{t2}}\right)^{\left(\frac{\gamma}{\gamma-1}\right)} \tag{17}$$

$$\rho_2 = \frac{P_2}{RT_2} \tag{18}$$

Blade loading and blockage factor at the outlet of the rotor are used to determine in an iterative manner, the number of blades and corresponding outlet blade angles:

$$\lambda = \frac{1}{1 - B_2} \tag{19}$$

where B_2 is a blockage factor of the flow area at the rotor tip. λ is calculated as:

$$\lambda = K_\lambda + \left(\frac{0.00175}{\phi}\right)^2 + \frac{0.0015}{\phi} - 0.22\ln(\phi) \tag{20}$$

The factor K_λ depends on several parameters. These include not only the blade angle β_b and passage area A at both inlet and outlet, but also the passage width b_2 at the outlet and the blade mean camber line length L_{UR}. L_{UR} and b_2 make the calculation procedure somewhat difficult since the blade camber line length and blade number Z_{UR} are unknown until the rotor geometry is determined:

$$K_\lambda = 1 + \left(0.3 + \left(\frac{b_2}{L_{b,UR}}\right)^2\right)\frac{b_2 A_2{}^2 \cos\beta_{b2}{}^2}{L_{b,UR} A_1{}^2 \cos\beta_{b1}{}^2} \tag{21}$$

$$b_2 = (1 - \frac{Z_{UR} t_b}{2\pi \cos\beta_{b2} r_2}) b_{2,SRCC} \tag{22}$$

$$L_B = \int_0^{L_{axUR}} \frac{m(z)}{\cos\beta_b(z)} dz \tag{23}$$

The blade angles distribution are implemented by using the following equations:

$$\beta_{bs} = \beta_{b1s} + (\beta_{b2} - \beta_{b1s})(3\zeta^2 - 2\zeta^3) \tag{24}$$

$$\beta_{bh} = \beta_{b1h} + A\zeta + B\zeta^2 + C\zeta^3 \tag{25}$$

$$A = -4(\beta_{b2} - \overline{\beta_h} + \beta_{b1h}) \tag{26}$$

$$B = 11\beta_{b2} - 16\overline{\beta_h} + 5\beta_{b1h} \tag{27}$$

$$C = -6\beta_{b2} + 8\overline{\beta_h} - 2\beta_{b1h} \tag{28}$$

$$\overline{\beta_h} = 90K + \frac{(1-K)(\beta_{b2} + \beta_{b1h})}{2} \tag{29}$$

$$\zeta = \frac{m_2 - m(z)}{m_2 - m_1} \tag{30}$$

$$m(z) = \int_0^z \sqrt{1 + \left[\frac{dr(z)}{dz}\right]^2} dz \tag{31}$$

$$m_2 = \int_0^{L_{axUR}} \sqrt{1 + \left[\frac{dr(z)}{dz}\right]^2} dz \tag{32}$$

Axial distance is calculated as:

$$L_{ax} = min(L_{ax,SRCC}, 2r_2[0.014 + 0.023r_2/r_{h1} + 1.58\phi]) \tag{33}$$

$m(z)$ is calculated numerically using Gauss method [25]. The range value of the parameter K is between $0-1$ to adjust the rake angle.

Finally, the wrap angle of blades is calculated as:

$$\theta(z) = \int_{m_1}^{m_2} \frac{\tan\beta_b(z)}{r(z)} dm(z) \tag{34}$$

$\theta(z)$ is initialized to have a zero value at the trailing edge at the hub (blade stacking condition) and adjusted at shroud to have the same rake angle as that of the SRCC impeller. Note that the blade number is calculated also by an inner iterative procedure. This design method is originally performed by a several iterative loops one in another to compute meridional and blades according to the limitation on blade loading defined. But in this study, the meridional shape is already known for both upstream and downstream rotors. The global blade loading is calculated from Ref. [19] as:

$$BL = \frac{\Delta W}{W_1 + W_2} \leq 0.9 \tag{35}$$

$$\Delta W = \frac{4\pi r_2 U_2 (I - I_{par})}{Z_{UR} L_{B,UR}} \tag{36}$$

Then, the tangential component of absolute velocity at the tip is recalculated (in an inner loop to determine λ) as:

$$\frac{C_{u2}}{U_2} = (I - I_{par}) = \sigma\left(1 - \frac{\lambda \dot{m} \tan\beta_{b2}}{\rho_2 A_2 U_2}\right) \tag{37}$$

σ is the slip factor. There are many empiric formulas for the slip model. The most recent one is given by Qiu et al. [26] and is employed. For simplicity and numerical stability, only the radial and turning terms in this model are implemented. The passage term is very small compared to other terms (see Ref. [26]) and difficult to implement. The design process is resumed as a flowchart shown in figure 4.

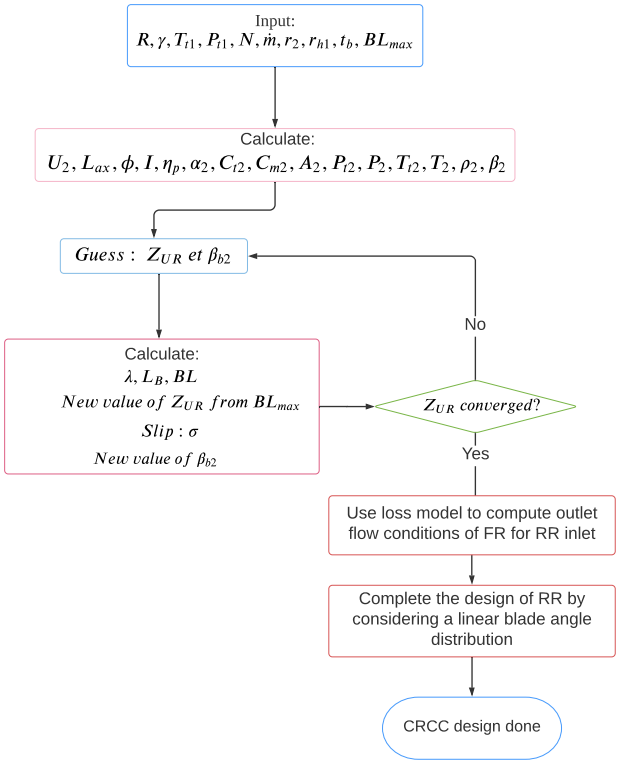

Fig. 4. CRCC design flowchart

Table 4. Performance comparison between four CRCC configurations by CFD calculations, $N_{UR} = -N_{DR} = 16000\,rpm$ at the design mass flow rate of $0.73\,kg/s$ [27]

Configuration	LR	Pressure ratio (s-s)	Polytropic efficiency (s-s)
C1	0.3	1.31	78%
C2	0.4	1.34	69%
C3	0.5	1.38	65%
C4	0.6	1.36	71%

Four values of LR are specified, and then four corresponding CRCC configurations are built by the design method described precedent at the design mass flow rate of $0.73\,kg/s$ with $N_{UR} = -N_{DR} = N_{SRCC} = 16000\,rpm$ [27]. These four CRCC configurations are analyzed by CFD and their performances in terms of pressure ratio and polytropic efficiency are shown in table 4.

The C1 configuration is therefore chosen to be manufactured because it delivers the highest efficiency and the closest pressure ratio to that of SRCC. Also, C1 aligns with the statement of Tosin et al. [28] in which they show that having the lowest value of LR (indirectly equivalent to the load factor) will give the highest efficiency machine. The geometric parameters of two counter-rotating rotors are resumed in table 5 and table 6. It can be noted that CRCC and SRCC have the same size and use the same volute to facilitate the performance evaluation. The structure of the test bench is presented in the figure 5.

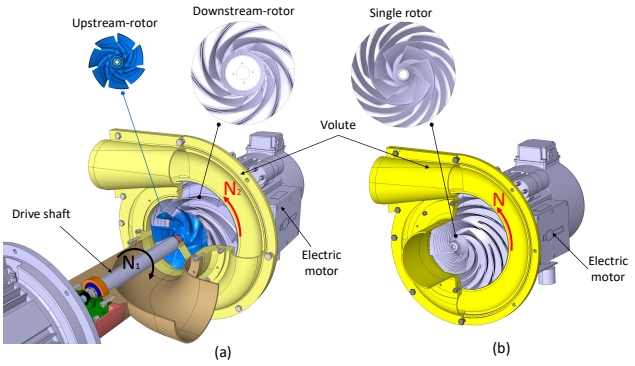

Fig. 5. Structure of a counter-rotating centrifugal compressor (CRCC) (a) and single rotor centrifugal compressor (SRCC) (b)

We discuss in this paper the first part of the experimental results of the CRCC global characteristics and compare them with those of the corresponding SRCC at the selected speeds, as shown in figure 2. It can be noted that the selected speed is lower than the design speed because of the electrical resource limitation.

3 Experimental setup

CRCC test bench works in suction application, the pressure outlet is the atmospheric pressure. Because CRCC uses two independent electric motors so its inlet form was changed by using a curved pipe type with an angle of 90°. The speed of two rotors: N_{UR} for the upstream-rotor and N_{DR} for the downstream-rotor, can vary independently by two inverters. The test platform consisted of a CRCC compressor connected to an open-loop system and driven by two independent electric motors. A locked valve located upstream of a storage tank is used to adjust the airflow into the system. The storage tank is then connected to a 3.5m long pipe to stabilize the flow. In the downstream of the compressor, a muffler was installed to reduce the noise of the system. The operating parameters of the compressor are measured by a sensor system that has been installed and described in figure 6. The mass flow rate is determined based on measuring pressure differentials on the Flo-Bar Averaging Pitot tube. The manometer FCO16 with an accuracy of $\pm 1\%$ was connected with the Pitot tube to measure the pressure differentials. The value of the mass flow rate is then calculated according to the calibration equation 38. Four Pt100 thermocouples with an accuracy in the range of $0.02° - 0.04°$ were used to determine the inlet and outlet temperatures. One thermocouple was placed at the inlet and three other ones were installed at the downstream pipe of the compressor. Four pressure taps distributed on the circumferential inlet tube were connected to a manometer FC332 with an accuracy of 0.5%, use to measure the average static pressure. Two Kisler 4005B highly sensitive instantaneous pressure sensors were used to measure the dynamic pressure in the system. By analyzing the dynamic pressure of these sensors, the fluctuations in pressure inside the system determine can be detected that determine the surge phenomenon. These two sensors are located in the inlet and the area between the two rotors.

Table 5. Upstream-rotor geometric parameters

Parameter	Value	Parameter	Value
d_{1h}	$59.5mm$	β_{b1h}	45.3°
d_{1sh}	$161mm$	β_{b1sh}	69.8°
d_{2h}	$118mm$	β_{b2h}	53.6°
d_{2sh}	$176mm$	β_{b2sh}	68.4°
N_{UR}	-16000 rpm	Z_{UR}	7
L_{UR}	31.9 mm		

Table 6. Downstream-rotor geometric parameters

Parameter	Value	Parameter	Value
d_{3h}	$128.5mm$	β_{b3h}	72.7°
d_{3sh}	$183mm$	β_{b3sh}	77°
d_4	$286mm$	β_{b4}	64°
N_{DR}	16000 rpm	Z_{DR}	9

$$\dot{m} = \frac{\pi D^2}{4} k \sqrt{2\rho\Delta P} \tag{38}$$

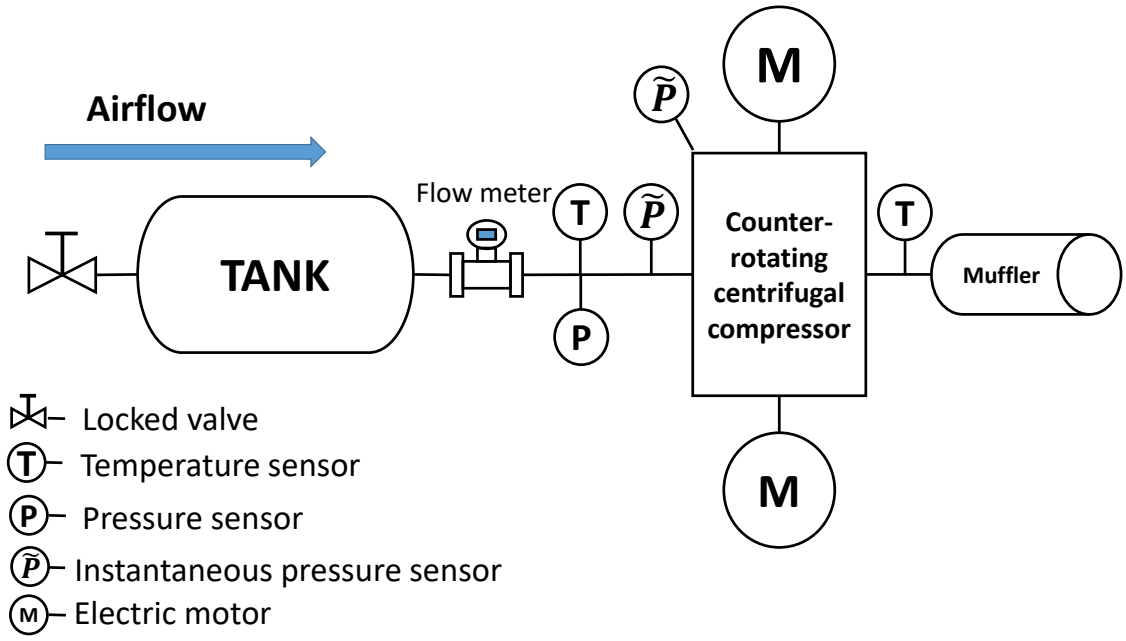

Fig. 6. Scheme of the counter-rotating centrifugal compressor (CRCC) test bench

To facilitate the comparison of the experimental results for different measurements, the calculated values of mass flow rate are referred to the same condition at $T_{ref} = 288.15\text{K}$ and $P_{ref} = 101,325Pa$, called corrected mass flow rate. This value is determined by the following equation:

$$\dot{m}_{cr} = \dot{m} \frac{\sqrt{\frac{T_1}{T_{ref}}}}{\frac{P_1}{P_{ref}}} \tag{39}$$

The pressure ratio is calculated by the static pressure at the inlet of the upstream-rotor and outlet of the volute and it is defined as:

$$\Pi_s = \frac{P_{atm}}{P_1} \tag{40}$$

The polytropic efficiency used in this study is calculated with the equation 41:

$$\eta_p = \frac{\gamma - 1}{\gamma} \frac{\ln\left(\frac{P_{atm}}{P_1}\right)}{\ln\left(\frac{T_{out}}{T_1}\right)} \tag{41}$$

4 Results and discussions

As mentioned above, CRCC uses two independent rotors, which means one more degree of freedom was added in the system as the speed of the second rotor. Increasing the degree of freedom of the compressor makes the design process more complicated. Therefore, it is essential to conduct experiments to explore the characteristics of the compressor type based on combining the speed of the rotors independently. Two cases of operation are considered for testing its impact on the CRCC performances.

Case 1: The upstream-rotor is freely rotated around its axis; the downstream-rotor rotates at a constant speed of $11k\,rpm$. In this case, the speed of the upstream-rotor depends on the mass flow rate through the compressor ($N_{UR} = f(\dot{m})$).

Case 2: The two rotors are driven simultaneously in the opposite directions ($N_{UR} = -N_{DR}$), called counter-rotating mode. The global performances of CRCC are then compared to that of SRCC at the same rotation speed of $11k\,rpm$.

4.1 Case 1- Behavior of CRCC with the upstream rotor is freely rotated

In this operating mode, the upstream-rotor is not driven by the electric motor, it rotates freely. The flow streamlines in figure 7 show how they pass the compressor. Due to the gradient-pressure between the compressor inlet and outlet, the fluid flow passes the upstream-rotor within the blade row. The high-velocity flow produces the gradient pressure on the rotor blade surface due to the airfoil shape of the rotor blade. The surface side with higher-pressure called Pressure Side (PS) and the other side with lower pressure called Suction Side (SS). The gradient pressure generates a torque which drives the upstream-rotor to rotate. It depends on the flow velocity or flow rate through the compressor. The rotational direction of this rotor is always contrary to the downstream-rotor direction. The flow out of the upstream-rotor was transferred energy by the downstream-rotor to accelerate and

compress. After that, it was delivered to the outlet pipe. As a result, the upstream-rotor works like a turbine. The energy consumes by this rotor decrease slightly the head of the compressor. The head rise of the CRCC is generated only by the work of the downstream-rotor.

Figure 8 illustrates the overall experimental characteristics of CRCC at three different speeds of $9k\,rpm$, $10k\,rpm$, $11k\,rpm$, and the free rotational speed of the upstream-rotor. It is easy to see that the speed of the upstream-rotor reduces according to a linear relation of the mass flow rate. The highest speed of the upstream-rotor achieves $-7.2k\,rpm$ when the lock valve opens maximum corresponding to a flow rate of 0.746kg/s. The speed of the upstream-rotor decreases gradually as the control lock valve closes continuously to diminish the flow into the compressor. It is no longer rotate at the mass flow of 0.191kg/s because at this flow rate the torque which is generate by the pressure differentials between PS and SS of the blades does not overcome the resistance torque of the drive system (figure 8a). It can be noted that the pressure ratio of the CRCC increases with increasing speed while the efficiency of the compressor is always stable at $72 \pm 1.2\%$ (figure 8b).

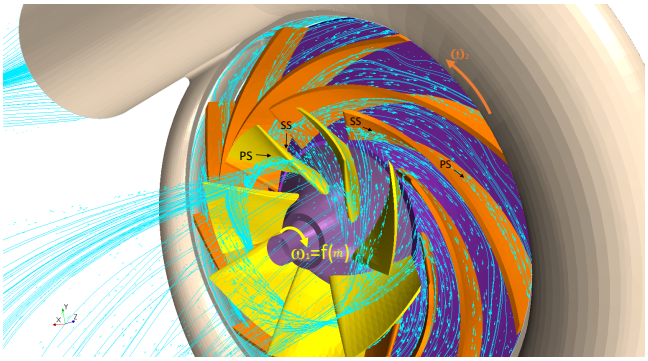

Fig. 7. The Pressure Side (PS) and Suction Side (SS) on the blade surfaces in case 1

On a wide range of flow rates, the CRCC exhibits slightly smaller pressure ratios than the SRCC at the observed speeds due to the energy dissipated in the upstream rotor. Nevertheless, for identical operating points based on pressure-flow rates, the CRCC demonstrates better efficiency every time than the SRCC. For example, for two points, P1 and P2, are marked in figure 9, the efficiency value goes, respectively, from 69±1.2% to 72,6±1.2% and 64±1.2% to 70±1.2%. This can be explained by the compatibility of the fluid flow with the rotors. When the upstream-rotor rotates freely, the fluid flow is well guided to the downstream-rotor. As a result, there is less loss by the inlet incidence. A downside, however, the operating points of the CRCC are obtained for slightly higher downstream-rotor rotation speeds ($10k\,rpm$ for CRCC and under $10k\,rpm$ for SRCC). The CRCC requires a higher speed to be able to achieve the same pressure ratio in this case because it has to compensate for the lost energy in the upstream rotor. For industrial applications, in case of the cost and space are considered, the upstream-rotor freely rotating rotor can be used as a pre-rotating inlet guide vane to improve the efficiency of the compressor.

4.2 Case 2 - Behavior of the CRCC with the upstream rotor motor powered

In this case, both rotors are driven simultaneously (counter-rotating mode). For this mode, the speed of the rotor can be the same or different. The ratio of the upstream-rotor speed to the downstream-rotor is defined as the speed ratio (θ) used to evaluate the compressor behavior. Firstly, the compressor behavior was analyzed at the same speed of $11k\,rpm$ (θ= 1). Next, the speed of the downstream-rotor is kept constant at three different speeds of $9k\,rpm$, $10k\,rpm$ and $11k\,rpm$; the speed of the upstream-rotor varies corresponding to the speed ratio changes in the range of [-0.7 -1.3].

4.2.1 Performance of CRCC at the speed ratio $\theta = -1$

Figure 10 presents the comparison of the global performance between CRCC (in counter-rotating mode) and SRCC at the speed of $11k\,rpm$. Obviously, the pressure ratio of CRCC is always higher than that of SRCC with the same tip-speed (figure 10a). It can be noted that the pressure deviation between CRCC and SRCC increases as the mass flow rate decreases. At the best efficiency point, the pressure ratio of CRCC is 1.194, which increases by about 4.6% compared to 1.141 of SRCC. It can be interpreted by the increase of the kinetic energy of the fluid flow. When the upstream-rotor is driven, the shaft power is transferred to the fluid flow lead to increase the relative velocity at the downstream rotor inlet. According to the velocity triangle as mentioned in section 2.1, the total enthalpy rise of CRCC increase due to the counter-rotating effect.

The comparison of polytropic efficiency between CRCC and SRCC is illustrated in figure 10b. It is clear that the CRCC efficiency is always higher than SRCC within the mass flow rate range of [0.4 0.7] kg/s. At the best efficiency point, the efficiency of CRCC increase by about 3.6% compared to SRCC. It can be remarked that this point is shifted to a lower mass flow rate at 0.584kg/s instead of 0.648kg/s for SRCC. However, the limit point of CRCC seems to be shifted to a higher mass flow rate. That means the surge phenomenon of CRCC appears early. This could be explained by the more sensitive incident angle at the downstream-rotor inlet. As stated by the velocity triangle, the inlet incidence angle increase quickly at the low flow rate due to the counter-rotating effect. Therefore, the separation region appears in the blade passage of the rotors and generates a stall cell. The instability appears when the stall cells are developed in the entire rotors.

Figure 10c shows the total power consumption of CRCC in comparison with the SRCC one. The red solid line and the green solid line represent the power consumption of the upstream-rotor CR(P1) and the downstream-rotor CR(P2), respectively. The black solid lines and black dashed lines are respectively the total power consumption of CRCC and

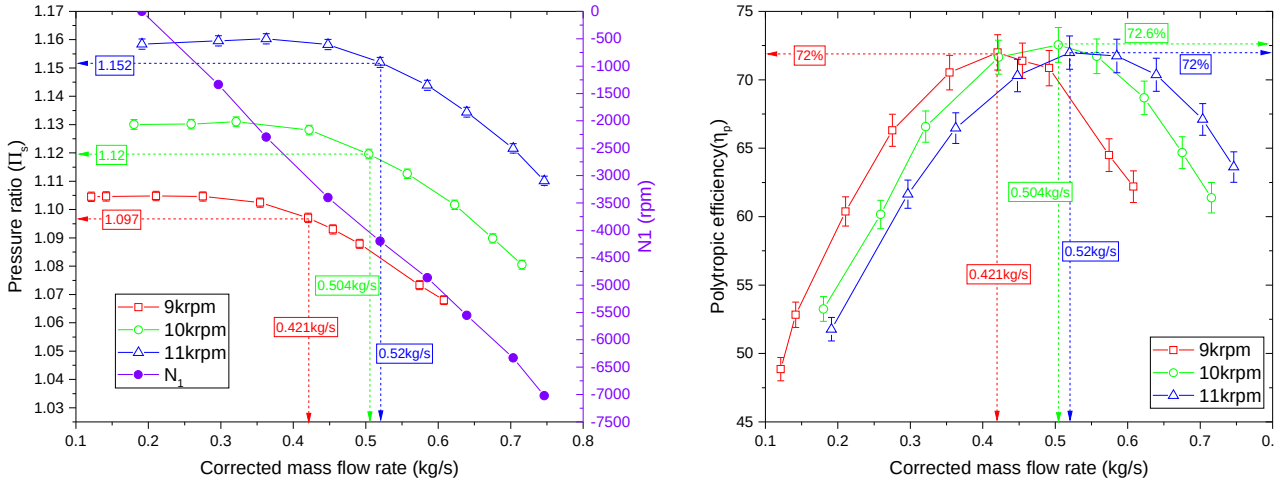

Fig. 8. Overall experimental-characteristics of CRCC at three speeds, $9k\,rpm$, $10k\,rpm$ and $11k\,rpm$ of downstream-rotor and in free-rotation of upstream-rotor: (a) Pressure ratio, upstream-rotor speed and (b) polytropic efficiency.

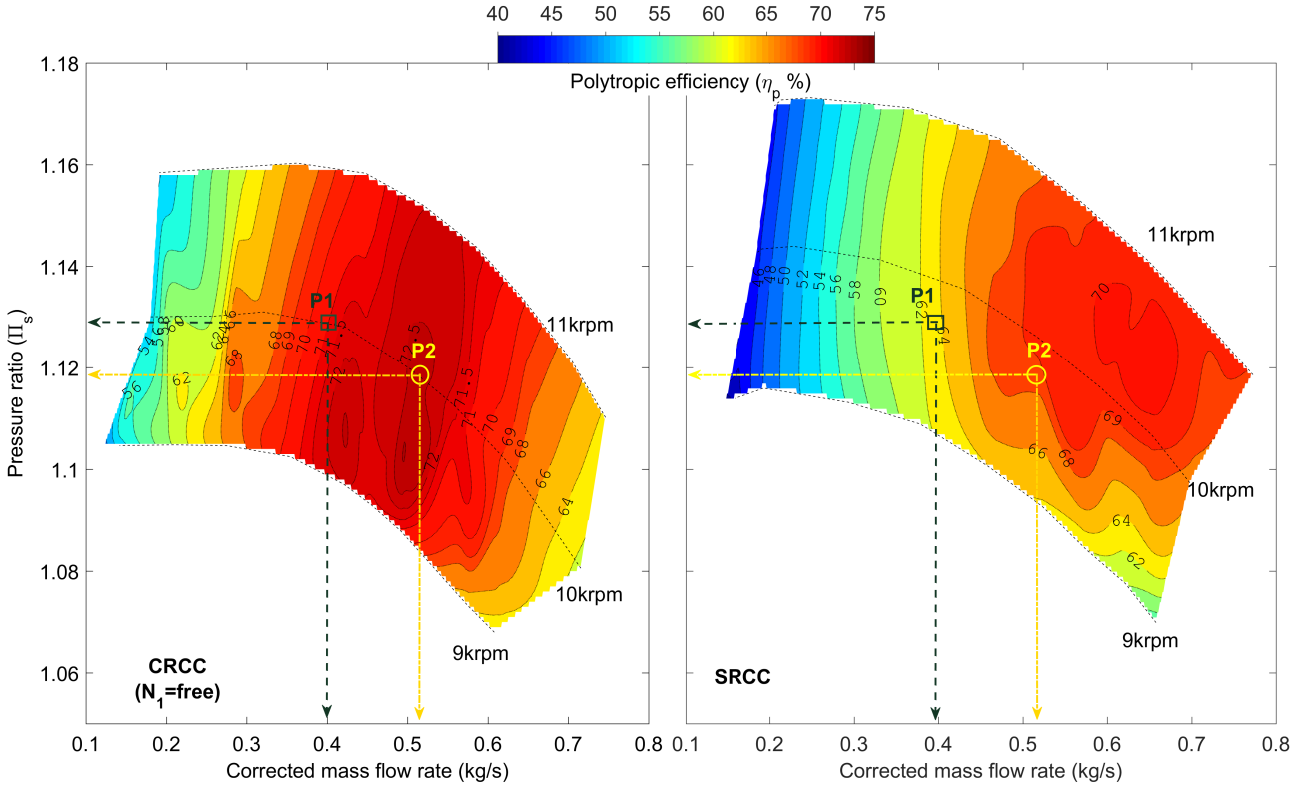

Fig. 9. Comparison of characteristics map between CRCC (left figure) and SRCC (right figure) at the three-rotation speed of $9k\,rpm$, $10k\,rpm$, and $11k\,rpm$

SRCC. It is easy to see the power consumption of the downstream-rotor is approximately equal to the power consumption of SRCC. This shows that the fluid is mainly compressed in the downstream-rotor because it has a large variable diameter from the inlet to the outlet. The consumption of the upstream-rotor is small and increases as the flow decreases, which is almost the characteristic of axial turbomachinery. Upstream-rotor mainly speeds up the fluid flow to the downstream-rotor. Consequently, the total power consumption of CRCC is always higher than that of SRCC because of the high-pressure rise and mechanical losses in the upstream-rotor drive system.

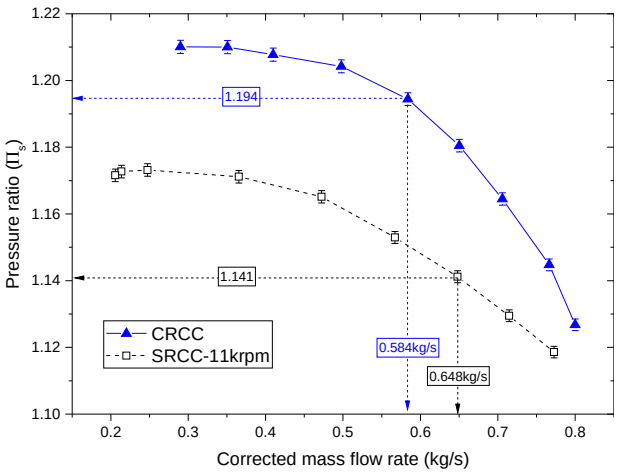

(a)

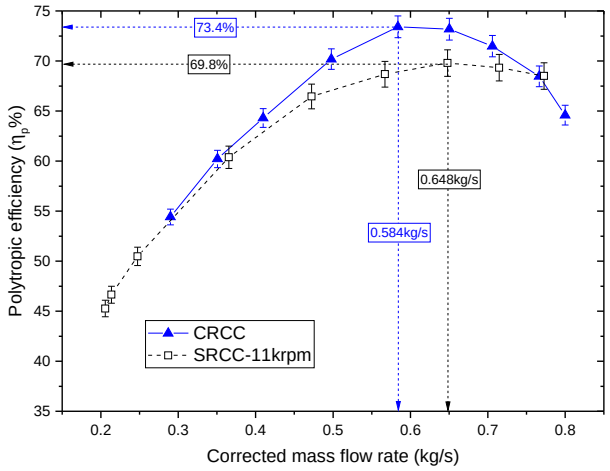

(b)

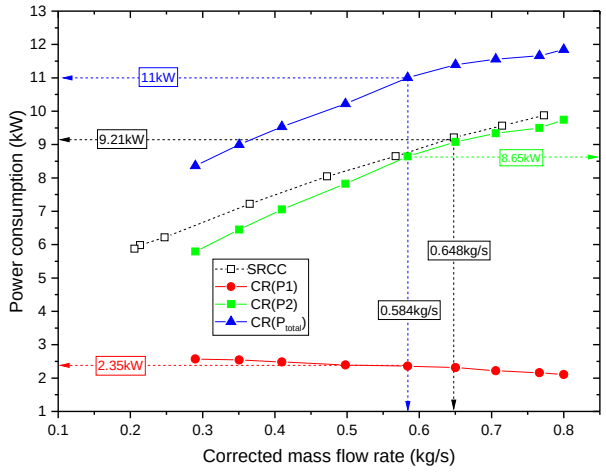

(c)

Fig. 10. Comparison of performance between CRCC in counter-rotating mode (case 2) and SRCC at the speed of $11k\,rpm$:(a) pressure ratio, (b) efficiency, and power consumption (c)

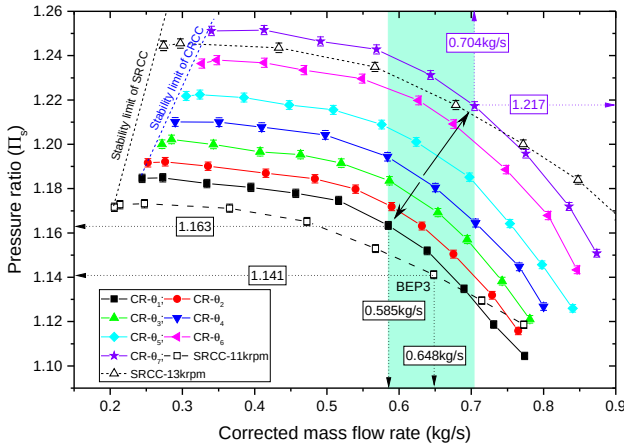

(a)

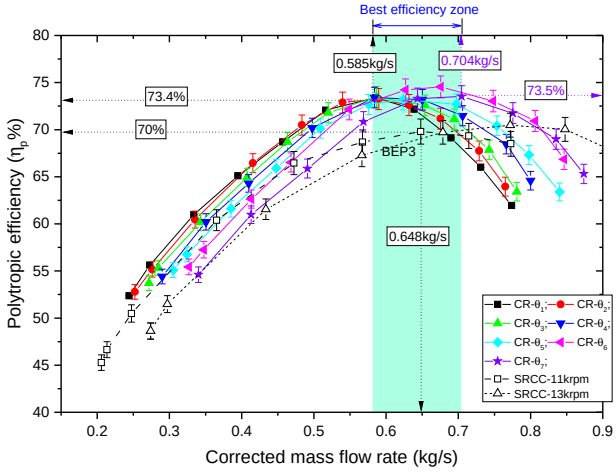

(b)

Fig. 11. Overall experimental-characteristics of CRCC with different speed ratios at the downstream-rotor speed of $11k\,rpm$: (a) pressure ratio and (b) efficiency

4.2.2 Influence of the speed ratio on the performance

The previous results illustrate the counter-rotating mode provides higher performance and produces more pressure ratio rise than SRCC at the same tip-speed. To investigate the effect of the speed ratio in the counter-rotating mode, the speed of the upstream-rotor varies with each fixed speed of the downstream-rotor. The variation of speed ratios is then conducted to evaluate its ability to reproduce the performance and the operating selected of SRCC at a lower tip-speed. The performance of SRCC is constructed at five main speeds of $9k\,rpm$, $10k\,rpm$, $11k\,rpm$, $12k\,rpm$, and $13k\,rpm$ as shown in figure 2. Three main speeds of the CRCC downstream-rotor of $9k\,rpm$, $10k\,rpm$ and $11k\,rpm$ are selected in this study. At each speed of the downstream-rotor, the speed of the upstream rotor varies corresponding to the speed ratio in a range of [-0.7 -1.3] (the minus sign represents two rotors rotating in the opposite directions). Seven speed-ratios of θ_1=-0.7, θ_2=-0.8, θ_3=-0.9, θ_4=-1, θ_5=-1.1, θ_6=-1.2 and θ_7=-1.3 are used to construct the characteristics of CRCC in order to the comparison. In this study, the results of the downstream-rotor speed at $11k\,rpm$ are illustrated to analyze the effect of speed ratio on the performance. Fig-

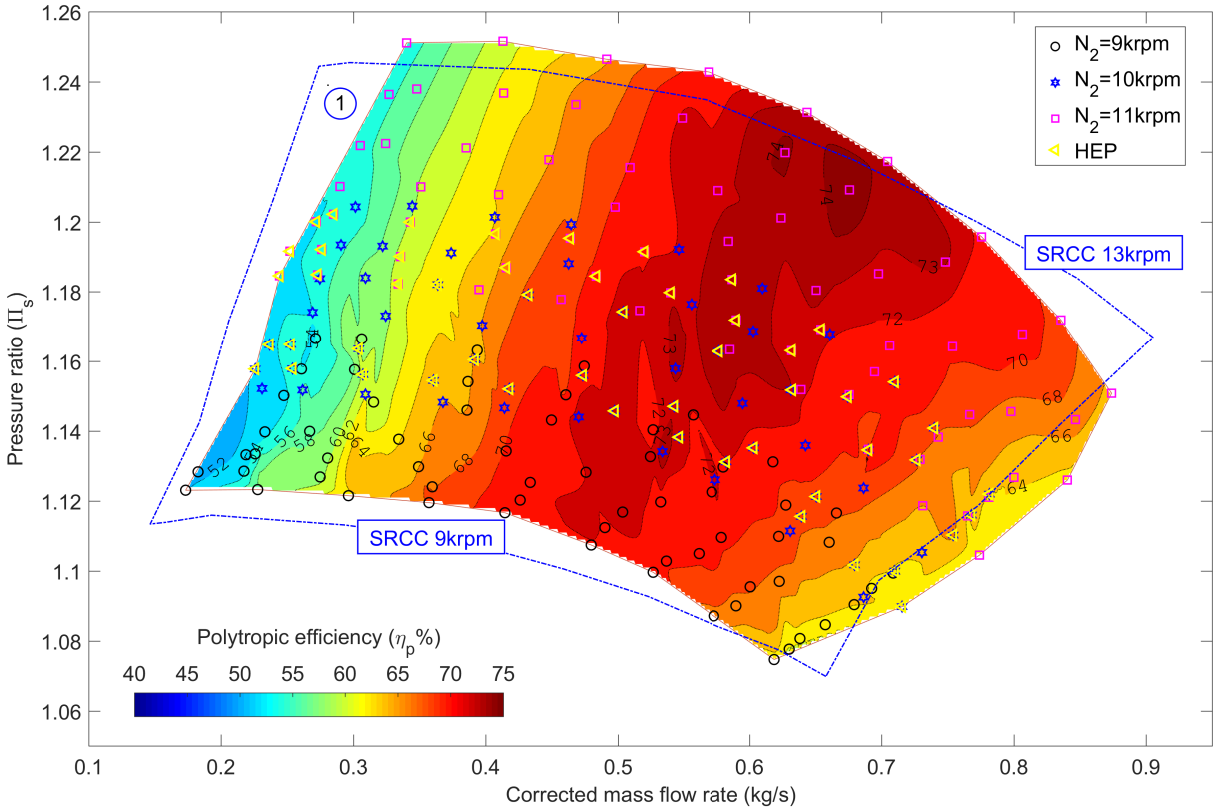

Fig. 12. Performance map of CRCC with $N_{DR} \in [9k\,rpm \quad 11k\,rpm]$, $N_{UR} \in [-6.3k\,rpm \quad -14.3k\,rpm]$

ure 11a shows the change of the pressure ratio characteristics when changing the speed ratio. It is obvious that the speed ratio has a strong effect on the pressure ratio. It decreases gradually if the speed ratio changes from θ_4=-1 to θ_1=-0.7 and increase rapidly if the speed ratio increases from θ_4=-1 to θ_7=-1.3. At the best efficiency point, the pressure ratio of CRCC reaches 1.163 with θ_1=-0.7 and goes up to 1.217 with θ_7=-1.3. In other words, the pressure ratio of CRCC increases from 1.9% up to 6.7% compared to that of SRCC at 1.141 if the speed ratio changes from θ_1=-0.7 to θ_7=-1.3. It must be pointed that the pressure ratio curve of CRCC with θ_7=-1.3 is almost equal to that of SRCC at the higher tip-speed by about $2k\,rpm$. Besides, the maximum efficiency of CRCC is almost unchanged, at 73.5±1.2%, as shown in figure 11b. It can be said that the efficiency of CRCC is improved by about 3.5% in comparison with the efficiency of SRCC of 70±1.2% at the same tip-speed. It should be observed that the best efficiency point attains at different mass flow rates. It moves according to the change of the speed ratio. This happens because at each speed-couples, there is only one point at which the fluid flow is well adapted for both rotors at a specific flow rate. Therefore, the compressor has the minimum loss. The set of the best efficiency points constitutes a best efficiency zone of CRCC. It is located between 0.585kg/s and 0.704kg/s with the change of the speed ratio. It should be recalled that the instability phenomenon of CRCC occurs early than the SRCC.

4.2.3 Map characteristics in counter-rotating mode

Two other speeds of the downstream-rotor of $9k\,rpm$ and $10k\,rpm$ are conducted with a similar method. The results of three speeds are then used to construct the characteristic map of CRCC as shown in figure 12. The contour of the SRCC map (blue dashed line) is also illustrated in this figure to compare with the CRCC one. It reveals that the operating range of the two compressors is almost the same. In addition, the high-efficiency region (red zone) of CRCC is broadened and becomes larger than that of SRCC (the comparison between figure 2 and figure 12). This region is shifted to a lower mass flow rate compared to SRCC's region. Furthermore, the higher efficiency region $\geq 70\%$ brown zone) can be seen clearly in the CRCC map. Besides, there are many ways to obtain the same pressure ratio characteristic in counter-rotating mode by simultaneously changing the speed of two rotors. In the selected speed, there are two regions where different speed ratios produce the overlap of the identical flow-pressure ratio curves. These curves have a slight difference in efficiency, and it depends on the

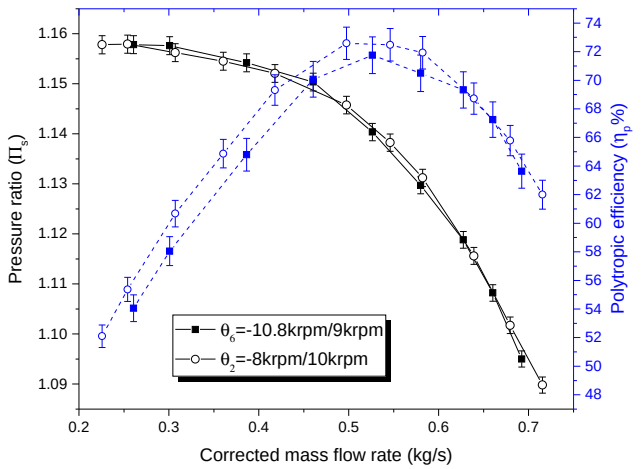

Fig. 13. Variation of efficiency between two speed ratios ($\theta_2 = -8k\,rpm/10k\,rpm = -0.8$ and $\theta_6 = -10.8k\,rpm/9k\,rpm = -1.2$) that give the identical flow-pressure ratio

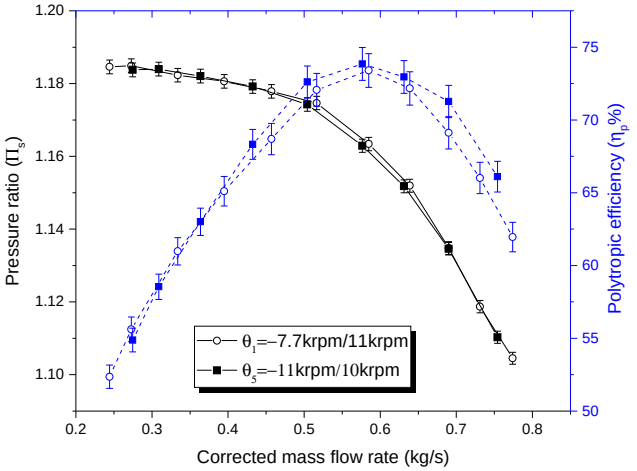

Fig. 14. Variation of efficiency between two speed ratios ($\theta_1 = -7.7k\,rpm/11k\,rpm = -0.7$ and $\theta_5 = -11k\,rpm/10k\,rpm = -1.1$) that give the identical flow-pressure ratio

speed of each rotor. The Higher Efficiency Points (HEP) are marked in figure 12 by selecting the higher efficiency point of two identical flow-pressure ratio curves. Two comparisons of efficiency between two identical flow-pressure ratio curves, for example, are shown in figure 13 and figure 14. In the first one, the efficiency curve of $\theta_2 = \frac{-8k\,rpm}{10k\,rpm} = -0.8$ is slightly higher than that of $\theta_6 = \frac{-10.8k\,rpm}{9k\,rpm} = -1.2$ (figure 13). The surge limit point has been shifted slightly towards the lower mass flow rate if the upstream-rotor speed is lower than the downstream-rotor. As a result, the efficiency can be improved with the same pressure ratio if the downstream-rotor speed is higher than the upstream-rotor speed. In contrast, the efficiency of $\theta_1 = \frac{-7.7k\,rpm}{11k\,rpm} = -0.7$ is a bit smaller than $\theta_5 = \frac{-11k\,rpm}{10k\,rpm} = -1.1$ in the second one (figure 14). Nonetheless, the surge limit point is always enhanced if the downstream-rotor rotates faster than the upstream-rotor. Consequently, CRCC can give almost the same characteristic as SRCC at lower tip-speeds and higher efficiency but the surge phenomenon occurs slightly earlier than SRCC.

5 Conclusions

In this paper, the design method based on the loss model was presented. This method permit determining the geometry of the rotors from a reference rotor which has the same dimensions. The results of this method were validated with the existing data base in the open literature. After that, an experiment was conducted to investigate the influence of the speed ratio on the performance of CRCC against SRCC. The results show that:

1. Case 1-Upstream-rotor rotates freely: CRCC can improve the efficiency up to 3.5% due to the fluid flow was well adapted to the rotors. The inlet loss was minimized in this case. However, the pressure ratio was slightly reduced because the energy loss to drive the upstream-rotor. It can be remarked that CRCC efficiency is always higher than SRCC at the same pressure ratio and flow rate but the tip-speed of CRCC increases slightly. In some case of industry application, it can be helpful to improve the compressor efficiency and the upstream-rotor works as a pre-rotating inlet guide vane.

2. Case 2 -The two rotors are driven simultaneously in the opposite directions ($N_{UR} = -N_{DR}$): CRCC can increase the pressure ratio up to 4.6% in comparison with SRCC at the same tip-speed. The polytropic efficiency is also improved by about 3.5%. The influence of the rotor speed on the performance of CRCC is then considered. The experimental results reveal that the speed ratio has a great influence on the pressure ratio of CRCC. The pressure ratio increases linearly with the speed ratio while the maximum efficiency seems to be stable. The pressure ratio can be increased up to 6.7% if the speed ratio goes up to -1.3. This can be explain by the increase of the flow kinetic energy which was provide by the upstream-rotor. It is worth noting that the best efficiency points of CRCC take place at the different mass flow rates when varying the speed ratio. At each speed-couples, the compressor has a minimum inlet loss at a specific flow rate due to the incidence angle modification according to the velocity triangles. The set of these points indicates the effective working area of CRCC. As a result, CRCC can give a more flexible operating range in comparison with SRCC to meet the various working conditions. Furthermore, CRCC can work at a lower tip-speed than SRCC to obtain the same performance and operating range.

However, the instability limit of CRCC is shifted to a higher mass flow rate. That means the surge occurs early in the CRCC configuration due to the higher sensitivity of the

downstream inlet incidence angle. Fortunately, this problem can be resolved by changing the speed and the rotation direction of the upstream-rotor to extend the operating range of the compressor. This content will be presented in other publication.

Declaration of Conflicting Interests

The author(s) declared no potential conflicts of interest with respect to the research, authorship, and/or publication of this article.

Acknowledgements

The authors would like to thank LIFSE laboratory, the Mauritanian and Vietnam governments with all support for this study. Special thanks to Sebastien PORCHERON, lab's engineer, for helping us assemble the test bench.

References

[1] Fukutomi, J., Shigemitsu, T., and Yasunobu, T., 2008. "Performance and internal flow of sirocco fan using contra-rotating rotors". *Journal of Thermal Science,* **17**(1), pp. 35–41.

[2] Tosin, S., Dreiss, A., and Friedrichs, J., 2015. "Exiperimental and numerical investigation of a counter-rotating mixed-flow single stage pump". *ASME expo 2015*, pp. 1–11.

[3] Sharma, P. B., Jain, Y. P., and Pundhir, D. S., 1988. "A study of some factors affecting the performance of a contra-rotating axial compressor stage". In Proceedings of the Institution of Mechanical Engineers, Part A: Journal of Power and Energy, Vol. 202, pp. 15–21.

[4] Furukawa, A., Shigemitsu, T., and Watanabe, S., 2007. "Performance test and flow measurement of contra-rotating axial flow pump". *Journal of Thermal Science,* **16**(1), pp. 7–13.

[5] Chen, Y. Y., Liu, B., Xuan, Y., and Xiang, X. R., 2008. "A study of speed ratio affecting the performance of a contra-rotating axial compressor". *Proceedings of the Institution of Mechanical Engineers, Part G: Journal of Aerospace Engineering,* **222**(7), pp. 985–991.

[6] Shi, L., Liu, B., Na, Z., Wu, X., and Lu, X., 2015. "Experimental investigation of a counter-rotating compressor with boundary layer suction". *Chinese Journal of Aeronautics,* **28**(4), pp. 1044–1054.

[7] Shigemitsu, T., Miyazaki, K., Hirosawa, K., Fukuda, H., et al., 2018. "Performance and internal flow of contra-rotating small-sized cooling fan". *Open Journal of Fluid Dynamics,* **8**(02), p. 181.

[8] Luo, D., Sun, X., and Huang, D., 2020. "Design of 1 + 1 / 2 counter rotating centrifugal turbine and performance comparison with two-stage centrifugal turbine". *Energy,* **211**, p. 118628.

[9] Mao, X., and Liu, B., 2020. "Investigation of the casing groove location effect for a large tip clearance in a counter-rotating axial flow compressor". *Aerospace Science and Technology,* **105**, p. 106059.

[10] Sun, S., Wang, S., Zhang, L., and Ji, L., 2021. "Design and performance analysis of a two-stage transonic low-reaction counter-rotating aspirated fan/compressor with inlet counter-swirl". *Aerospace Science and Technology,* **111**, p. 106519.

[11] Price, N. C., 1941. Counterrotating supercharger. US2344366A.

[12] Florjancic, D., and Riedler, J., 19891. Kreiselmaschine mit gegenlufigen laufrdern und verwendung der kreiselmaschine. EP0348342A1.

[13] Dejour, Q., and Vo, H. D., 2018. "Assessment of a novel non-axial counter-rotating compressor concept for aero-engines". In ASME Turbo Expo 2018: Turbomachinery Technical Conference and Exposition, American Society of Mechanical Engineers Digital Collection.

[14] Limin, G. A. O., Xiaojun, L. I., Jian, X., and Bo, L. I. U., 2012. "The Effect of Speed Ratio on the First Rotating Stall Stage in Contra-Rotating Compressor". In Turbine Technical Conference and Exposition, Vol. 8, pp. 207–216.

[15] Mistry, C., and Pradeep, A. M., 2013. "Effect of variation in axial spacing and rotor speed combinations on the performance of a high aspect ratio contra-rotating axial fan stage". *Proceedings of the Institution of Mechanical Engineers, Part A: Journal of Power and Energy,* **227**(2), pp. 138–146.

[16] Nouri, H., Danlos, a., Ravelet, F., Bakir, F., and Sarraf, C., 2013. "Experimental Study of the Instationary Flow Between Two Ducted Counter-Rotating Rotors". *Journal of Engineering for Gas Turbines and Power,* **135**(2), p. 022601.

[17] Subbarao, R., and Govardhan, M., 2014. "Effect of speed ratio on the performance and flow field of a counter rotating turbine". In Energy Procedia, Vol. 54, pp. 580–592.

[18] Oh, H. W., Yoon, E. S., and Chung, M., 1997. "An optimum set of loss models for performance prediction of centrifugal compressors". *Proceedings of the Institution of Mechanical Engineers, Part A: Journal of Power and Energy,* **211**(4), pp. 331–338.

[19] Aungier, R. H., 2000. *Centrifugal compressors: a strategy for aerodynamic design and analysis*. American Society of Mechanical Engineers.

[20] Casey, M., Zwyssig, C., and Robinson, C., 2010. "The cordier line for mixed flow compressors". In Turbo Expo: Power for Land, Sea, and Air, Vol. 44021, pp. 1859–1869.

[21] Pakle, S., and Jiang, K., 2018. "Design of a high-performance centrifugal compressor with new surge margin improvement technique for high speed turbomachinery". *Propulsion and Power Research,* **7**(1), pp. 19–29.

[22] BOURABIA, L., ABED, C. B., CERDOUN, M., KHALFALLAH, S., DELIGANT, M., KHELLADI, S., and CHETTIBI, T., 2021. "Aerodynamic prelim-

inary design optimization of a centrifugal compressor turbocharger based on a one-dimensional mean-line model". *Engineering Computations*.

[23] Deligant, M., Sauret, E., Persky, R., Khelladi, S., and Bakir, F., 2018. "3d cfd simulation of a turbocharger compressor used as a turbo expander for organic rankine cycle".

[24] McKain, T. F., and Holbrook, G. J., 1997. Coordinates for a high performance 4:1 pressure ratio centrifugal compressor.

[25] Robert, R., BAKIR, F., and POULAIN, J., 2012. "Pompes rotodynamiques-similitude et conception des pompes centrifuges".

[26] Qiu, X., Japikse, D., Zhao, J., and Anderson, M. R., 2011. "Analysis and validation of a unified slip factor model for impellers at design and off-design conditions". *Journal of Turbomachinery,* **133**(4), p. 041018.

[27] Nguyen, V. T., Danlos, A., Paridaens, R., and Bakir, F., 2019. "Study of the Effect of the Contra-Rotating Component on the Performance of the Centrifugal Compressor". *International Journal of Mechanical, Industrial and Aerospace Sciences,* **12.0**(5), Apr.

[28] Tosin, S., Friedrichs, J., Farooqi, R., and Dreiss, A., 2014. "New approach for multi-rotor mixed-flow pump design and optimization". In ASME 2014 4th Joint US-European Fluids Engineering Division Summer Meeting collocated with the ASME 2014 12th International Conference on Nanochannels, Microchannels, and Minichannels, American Society of Mechanical Engineers Digital Collection.